Polyhedron 70 (2014) 71–76

Contents lists available at ScienceDirect

Polyhedron

journal homepage: www.elsevier.com/locate/poly

Crystal structure and properties of the precursor $[Ni(H_2O)_6](HTBA)_2{\cdot}2H_2O$ and the complexes $M(HTBA)_2(H_2O)_2$ (M = Ni, Co, Fe)

Nicolay N. Golovnev [a], Maxim S. Molokeev [b,*], Sergey N. Vereshchagin [c], Victor V. Atuchin [d,e], Maxim Y. Sidorenko [a], Michael S. Dmitrushkov [a]

[a] Department of Chemistry, Siberian Federal University, Svobodny Ave. 79, Krasnoyarsk 660041, Russia
[b] Laboratory of Crystal Physics, Kirensky Institute of Physics, SB RAS, Akademgorodok 50-38, Krasnoyarsk 660036, Russia
[c] Laboratory of Catalytic Conversion of Small Molecules, Institute of Chemistry and Chemical Technology, SB RAS, Krasnoyarsk 660036, Russia
[d] Laboratory of Optical Materials and Structures, Institute of Semiconductor Physics, SB RAS, Novosibirsk 630090, Russia
[e] Tomsk State University, Tomsk 634050, Russia

ARTICLE INFO

Article history:
Received 22 October 2013
Accepted 11 December 2013
Available online 29 December 2013

Keywords:
2-Thiobarbiturate complexes
3D elements
Synthesis
Structure
IR spectra
Thermal stability

ABSTRACT

Four new compounds, the discrete complex $[Ni(H_2O)_6](HTBA)_2{\cdot}2H_2O$ (**1**) and the polymers $Ni(H_2O)_2(HTBA\text{-}O,S)_2$ (**2**), $Co(H_2O)_2(HTBA\text{-}O,S)_2$ (**3**) and $Fe(H_2O)_2(HTBA\text{-}O,S)_2$ (**4**) (H_2TBA = 2-thiobarbituric acid, $C_4H_4N_2O_2S$), have been synthesized and structurally characterized. The structure of **1** has been solved by X-ray single-crystal diffraction analysis. The $Ni(H_2O)_6^{2+}$ cation has an almost ideal octahedral geometry, and there is no coordination of Ni(II) by $HTBA^-$ in **1**. Complexes **2**–**4** have been characterized by powder XRD, TG-DSC and FT-IR. In the isostructural polymers **2**–**4**, the metals are six-coordinated, and the octahedrons are connected by μ_2-O,S bridging ligands. Each of the M(II) ions is surrounded by two water molecules, two O-coordinated $HTBA^-$ ions and two S-coordinated $HTBA^-$ ions, with all pairs being in *trans*-positions. Hydrogen bonding and π–π interactions play an important role for the construction of the supramolecular 3D structures of **2**–**4**. The formation of the complexes has been evidenced by infrared spectroscopy. The thermal decomposition of **2**–**4** under oxidative conditions has been divided into three major stages: dehydration, oxidative degradation of the organic moiety and transformation of the inorganic residue.

1. Introduction

The coordination chemistry of heterocyclic thione ligands has developed rapidly due to their fascinating structural diversity and potential applications [1]. 2-Thiobarbituric acid (H_2TBA, $C_4H_4N_2O_2S$) has been widely studied, and the compound belongs to a very important class of pharmacological barbiturates [2]. It is a multifunctional ligand and, for instance, the acid shows desirable properties in forming different polymeric structures. Coordination polymers with organic linkers based on transition metals are of particular interest because of their intriguing topology and promising applications in adsorption, catalysis and separation [3–5]. These factors make the synthesis of d-element coordination polymers a strategic challenge. The fundamental aim of the present study is to trace the changes in the solid-state structures of thiobarbiturate complexes induced by transition metal substitution. Four new compounds, the discrete complex $[Ni(H_2O)_6](HTBA)_2{\cdot}2H_2O$ (**1**) and the polymers $Ni(H_2O)_2(HTBA\text{-}O,S)_2$ (**2**), $Co(H_2O)_2(HTBA\text{-}O,S)_2$ (**3**) and $Fe(H_2O)_2(HTBA\text{-}O,S)_2$ (**4**) (Fig. 1S), were synthesized and structurally characterized. Herein, we report the results on the synthesis, solid state structure, IR spectra and thermal decomposition of these new compounds.

2. Experimental

2.1. General methods

2-Thiobarbituric acid [CAS 504-17-6] was commercially available from Fluka. $FeSO_4{\cdot}7H_2O$ and basic carbonates of nickel(II) and cobalt(II) were obtained as reagent grade materials, and they were used without further purification. The IR absorption spectra of the compounds over the range of 400–4000 cm^{-1} were recorded at room temperature on a VECTOR 22 Fourier spectrometer. The chemical analysis was carried out with an HCNS-0 EA 1112 Flash Elemental Analyser. The simultaneous thermal analysis (STA) measurements were performed in a Netzsch STA Jupiter 449C with an Aeolos QMS 403C mass-spectrometer under a dynamic argon-oxygen

* Corresponding author. Tel.: +7 (391)2494507.
E-mail address: msmolokeev@gmail.com (M.S. Molokeev).

0277-5387/$ - see front matter © 2013 Elsevier Ltd. All rights reserved.
http://dx.doi.org/10.1016/j.poly.2013.12.021

atmosphere (20% O_2, 50 ml min^{-1} total flow rate). Platinum crucibles with perforated lids were used and the sample mass taken for the STA experiments was in the range 4.2–4.8 mg. A typical measurement procedure consisted of a temperature stabilization segment (30 min at 40 °C) and a dynamic segment at a heating rate of 10 K min^{-1}. The qualitative composition of the gases evolved was determined by on-line QMS in the Multiple Ion Detection mode. The following predefined ions were scanned: m/z = 18 (H_2O), 28 (N_2, CO), 30 (NO), 32 (O_2), 44 (CO_2), 64 (SO_2).

2.2. Synthesis of complexes **1–4**

Complexes **1**-**3** were readily prepared by the neutralization of 2-thiobarbituric acid with the corresponding basic metal carbonate in the aqueous solution. The neutral complexes **2** and **3** were prepared according to the following general procedure. The ligand (2 mmol) was mixed with an abundance of the basic metal carbonate in water (50 cm^3). The mixture was stirred for 5 h at 60 °C, and then filtered. Yellow crystals of **2** and lilac crystals of **3**, suitable for X-ray powder diffraction analysis, were grown by continuous filtrate evaporation at room temperature. Blue single crystals of **1** precipitated in the solution of the precursor of **2** at 5–20 °C, which quickly decomposed into the yellow powder of $Ni(H_2O)_2(HTBA)_2$ (**2**) in the air or aqueous solution. The powder of **4** was prepared by the following method. A solution of $FeSO_4{\cdot}7H_2O$ (1 mmol) in water (25 cm^3) was mixed with solid H_2TBA (2 mmol), and then the suspension was slowly neutralized at pH 7.0 using 0.1 M sodium hydroxide solution. The resulting mixture was stirred until the formation of a white precipitate. All the powders were removed by filtration, washed with acetone and dried in the air.

Anal. Calc. for $C_8H_{10}N_4NiO_6S_2$: C, 25.2; H, 2.64; N, 14.7; S, 16.8. Found: C, 24.8; H, 2.76; N, 14.3; S, 16.3%. *Anal.* Calc. for $C_8H_{10}CoN_4O_6S_2$: C, 25.2; H, 2.64; N, 14.7; S, 16.8. Found: C, 25.4; H, 2.70; N, 14.4; S, 16.8%. *Anal.* Calc. for $C_8H_{10}FeN_4O_6S_2$: C, 25.4; H, 2.67; N, 14.8; S, 17.0. Found: C, 25.3; H, 2.72; N, 14.6; S, 16.8%.

2.3. Single crystal X-ray diffraction analysis

The determination of the unit cell and the data collection for **1** were performed on a Bruker SMART APEX II diffractometer with graphite-monochromated Mo Kα radiation (λ = 0.71073 Å) using the ω–2θ scan technique. The crystal was placed in a capillary with the solution to prevent its decomposition. The structure was solved by direct methods using SHELXS-97 [6] and refined against F^2 by full matrix least-squares using SHELXL-97. All non-hydrogen atoms were refined anisotropically. All hydrogen atoms were positioned by difference Fourier maps and the thermal parameters set equal to 1.2 Ueq of the parent atoms. All hydrogen atoms of $HTBA^-$ were refined using a riding model with restraints. All water hydrogen atoms were refined at a distance restraint of d(O–H) = 0.90(3) Å. A summary of the crystal data, experimental details and refinement results are reported in Table 1. Selected bond lengths determined for **1** are listed in Table 1S. The intermolecular hydrogen bonds are summarized in Table 2S.

2.4. Powder X-ray diffraction analysis

The blue single crystals of **1** quickly decompose into the yellow powder $Ni(H_2O)_2(HTBA)_2$ (**2**) in the air. $Co(H_2O)_2(HTBA)_2$ (**3**) and $Fe(H_2O)_2(HTBA)_2$ (**4**) were also synthesized in powder forms, and their crystal structures were refined by the Rietveld method. The powder X-ray diffraction (XRD) data were collected on a Bruker D8 ADVANCE Bragg-Brentano diffractometer with the linear detector VANTEC using Cu Kα radiation. The beam was controlled by a 0.6 mm fixed divergence slit, 6 mm receiving VANTEC slit and Soller slits. The variable counting time (VCT) and step size (VSS) scheme were used to collect the diffraction data. The measurement time was systematically increased towards higher 2θ angles, leading to drastically improved data quality [7–9]. As a rule, 5–8 data points should be measured over the full-width-at-half-maximum. However, the peaks are significantly broadened for increasing 2θ. Therefore, for high 2θ angles, the step size should be increased to avoid wasting measurement time [10].

To collect the X-ray data from **2**, **3** and **4** at 296 K using the VCT scheme, four angle ranges were generated in the diffraction pattern: (1) 2θ range 5–38.7°, step 0.016°, 75.8 sec per step; (2) 2θ range 38.7–60.0°, step 0.024°, 227.4 sec per step; (3) 2θ range 60.0–97.5°, step 0.032°, 379 sec per step and (4) 2θ range 97.5-140°, step 0.040°, 758 sec per step. The total experimental time was equal to 19.2 h for each crystal. Further, the data were

Table 1
Crystallographic data for all the structures.

	1	**2**	**3**	**4**
Empirical formula	$C_8H_{26}N_4NiO_{14}S_2$	$C_8H_{10}N_4NiO_6S_2$	$C_8H_{10}CoN_4O_6S_2$	$C_8H_{10}FeN_4O_6S_2$
Crystal size (mm^3) or form	0.3 × 0.3 × 0.2	powder	powder	powder
Color	blue	yellow	pink	white
Molecular mass	525.16	381.03	381.27	378.19
Crystal system	triclinic	triclinic	triclinic	triclinic
Space group	$P\bar{1}$	$P\bar{1}$	$P\bar{1}$	$P\bar{1}$
a (Å)	7.389(6)	6.8817(4)	6.8922(4)	6.8761(3)
b (Å)	7.631(6)	7.0516(5)	7.0384(4)	7.0863(4)
c (Å)	10.082(8)	7.1907(4)	7.2536(3)	7.2772(3)
α (°)	101.278(8)	91.084(3)	91.499(2)	91.174(2)
β (°)	96.786(8)	103.514(3)	102.659(2)	102.687(2)
γ (°)	108.066(8)	113.128(2)	113.512(1)	113.471(1)
V ($Å^3$)	520.2(7)	309.61(3)	312.27(3)	314.99(3)
Z	1	1	1	1
T (K)	296(2)	296	296	296
Calculated density (g cm^{-3})	1.676	2.043	2.027	1.994
F(000)	1833	194	193	192
Reflections collected	5052	1177	1185	1211
Independent reflections	2698	–	–	–
Data/restrains/parameters	2698/10/164	1177/0/110	1185/0/110	1211/0/110
Goodness-of-fit	1.028	2.153	1.130	1.239
Final R indices [$I > 2\sigma(I)$] (%)	R_1 = 4.67	–	–	–
	wR_2 = 15.11	–	–	–
R indices (all data) (%)	R_1 = 6.16	R_p = 1.050, R_B = 0.33	R_p = 0.412, R_B = 0.120	R_p = 0.684, R_B = 0.231
	wR_2 = 16.60	R_{wp} = 0.995	R_{wp} = 0.383	R_{wp} = 0.648

Table 2
Thermal decomposition data of $M(H_2O)_2(HTBA)_2$ (M = Fe, Co, Ni). T_i, onset of initial decomposition temperature; T_m, DTG peak temperature; Δm_{obs} and Δm_{clc}, observed and calculated weight-loss value at each decomposition step. Dynamic atmosphere Ar–O_2 (80/20 by volume), 10 K min^{-1}.

Compound	Decomposition				
	T_i (°C)	T_m (°C)	Δm_{obs} (%)	Δm_{clc} (%)	Product
$Fe(H_2O)_2(HTBA)_2$	~130	261	13.2	9.52	$Fe(HTBA)_2$*
	~300	381	52.9		
	448	457	73.4		
	~525	606	78.93	78.88	Fe_2O_3
$Co(H_2O)_2(HTBA)_2$	~160	253	11.2	9.44	$Co(HTBA)_2$*
	~290	410	54.9		
	~470	530	72.7		
	~661	747	78.02	78.95	Co_3O_4
	911	920	79.48	80.35	CoO
$Ni(H_2O)_2(HTBA)_2$	210	273	11.4	9.45	$Ni(HTBA)_2$*
	~306	(375)	(49)		
	~464	510	76.38		
	640	713	79.80	80.39	NiO

* Expected product.

converted to the standard XYE files containing coordinates $2\theta_i$, intensity I_i and standard deviation $\sigma(I_i)$ for each point. The Rietveld refinement was produced using TOPAS 4.2 [11] and accounting for the standard deviation by implementing weight $w_i = 1/\sigma(I_i)^2$ for each point. The X-ray pattern of **2** was indexed in the triclinic $P\bar{1}$ (or *P1*) space group with $a = 6.8755$ Å, $b = 7.0431$ Å, $c = 7.1809$ Å, $\alpha = 88.90°$, $\beta = 103.53°$, $\gamma = 66.92°$ (Gof = 22.11), the X-ray pattern of **3** was indexed in the triclinic $P\bar{1}$(or *P1*) space group with $a = 6.8798$ Å, $b = 7.0446$ Å, $c = 7.2553$ Å, $\alpha = 88.49°$, $\beta = 103.61°$, $\gamma = 66.50°$ (Gof = 11.85), and the X-ray pattern of (**4**) was also indexed in the triclinic $P\bar{1}$ (or *P1*) space group with $a = 6.8708$ Å, $b = 7.0830$ Å, $c = 7.2736$ Å, $\alpha = 88.82°$, $\beta = 102.69°$, $\gamma = 66.520°$ (Gof = 45.9) using the program TOPAS 4.2. Therefore, the structures of **2**, **3** and **4** are isostructural. The cell parameters were converted to the conventional form by the program PLATON [12].

The crystal structures of **2**, **3** and **4** were solved in the $P\bar{1}$ space group using direct space modelling and the simulated anneal method in TOPAS 4.2. Further Rietveld refinement performed in TOPAS without any constrains was stable and led to low R-factors (Figs. 2S, 3S, 4S; Table 1). In these structures, all the H atoms of the $HTBA^-$ anions were not refined and were positioned geometrically. Missing water H atom positions were not refined and were calculated on the basis of potential hydrogen bonds (Table 2S). The thermal parameters of Ni, Co and Fe were refined anisotropically, all non-H atoms were refined isotropically, and thermal parameters of all H atoms were not refined. Selected bond lengths determined in **2**, **3** and **4** are listed in Table 1S.

3. Results and discussion

3.1. Crystal structure of *1*

The results of the X-ray single crystal diffraction experiment reveal a discrete structure for complex **1**. The asymmetric unit of the hexaaquanickel(II) bis(2-thiobarbiturate) dihydrate, $[Ni(H_2O)_6](HTBA)_2]\cdot 2H_2O$, consists of one half Ni(II) center, one $HTBA^-$ and five water molecules. The Ni(II) ion is coordinated by six oxygen atoms from water molecules, forming an almost ideal NiO_6 octahedron. The Ni–O bond distances range from 2.028(3) to 2.053(3) Å, which is comparable to those reported for Ni–O (carbonyl) and Ni–O (aqua) bonds in other six-coordinate nickel complexes [13]. The octahedra are isolated. There is no coordination of Ni(II) by $HTBA^-$, therefore this compound is a precursor of **2**. The C6–O2 distance [1.272(4) Å] is almost equal to the C4–O1 [1.268(4)] distance, being within one standard deviation (Table 1S), and this indicates charge delocalization in the $HTBA^-$ ligand. The C4–C5–C6 angle [120.3(2)°] corresponds to sp^2 hybridization. Also, the C4–C5 and C5–C6 distances [1.388(3), 1.391(3) Å] are close to the values typical of aromatic ring construction. The C2–S distance [1.639(9) Å] is comparable to those reported for a C=S double bond in thiobarbiturate compounds and is shorter than the theoretical value of a C–S single bond (1.78 Å). Other geometric parameters of the $HTBA^-$ ion are also in good relation with those of thiobarbituric [14,15] acid and other known free thiodarbiturates [16–21].

Hydrogen bonding, Fig. 5S, plays an important role in **1**. Twelve hydrogen bonds (Table 2S) generate a three-dimensional net. The hydrogen bonds N1–H1···O2 and N3–H3···O1 close 6-membered rings, with the graph set notation of the rings being described as $R_2^2(8)$. The hydrogen bonds O7–H7A···O4 and O7–H7B···O4 close 8-membered rings [$R_4^2(8)$], like O6–H6A···S and O6–H6B···S bonds and O3–H3A···O7 and O3–H3B···O7 bonds. In compound **1**, there is not π–π stacking interaction between the $HTBA^-$ rings, because the minimum perpendicular distance between the rings of neighboring $HTBA^-$ ions is 4.009(4) Å. The powder pattern of **1** could not be measured as its lifetime in the air is less than half an hour.

3.2. Crystal structures of *2*, *3* and *4*

The neutral complexes *catena*-bis(2-thiobarbiturato)diaquanickel(II), $Ni(H_2O)_2(HTBA)_2$ (**2**), *catena*-bis(2-thiobarbiturato)diaquacobalt(II), $Co(H_2O)_2(HTBA)_2$ (**3**), *catena*-bis(2-thiobarbiturato) diaquairon(II), $Fe(H_2O)_2(HTBA)_2$ (**4**) and *catena*-bis(2-thiobarbiturato)diaquacadmium(II), $Cd(H_2O)_2(HTBA)_2$ [21] are isostructural. The dependence of the cell volume on the ion radius of M^{2+} [22] for **2**, **3**, **4** and $Cd(H_2O)_2(HTBA)_2$ shows good the linear function shown in Fig. 6S. Contrary to **1**, they form polymer structures. The asymmetric unit consists of one half M^{2+} (M = Fe, Co, Ni) ion, one $HTBA^-$ ion and one coordinated water. Each M(II) ion is surrounded by two water molecules, two O-connected $HTBA^-$ ions and two S-connected $HTBA^-$ ions, and all pairs are in *trans*-positions (Fig. 2a–c). Therefore, in **2**, the Ni(II) ion is coordinated by the $HTBA^-$ ion, contrary to **1**. The $HTBA^-$ ion plays the role of a bridge between polyhedrons and forms a chain in the direction of the *c* axis (Fig. 7S). Compound **1** can be regarded as a precursor for complex **2**, where the HTBA ions are not directly connected with the Ni(II) ion, but are located in the outer coordination sphere of **1**. They interact with the complex cation $[Ni(H_2O)_6]^{2+}$ electrostatically, and they also form hydrogen bonds with coordinated

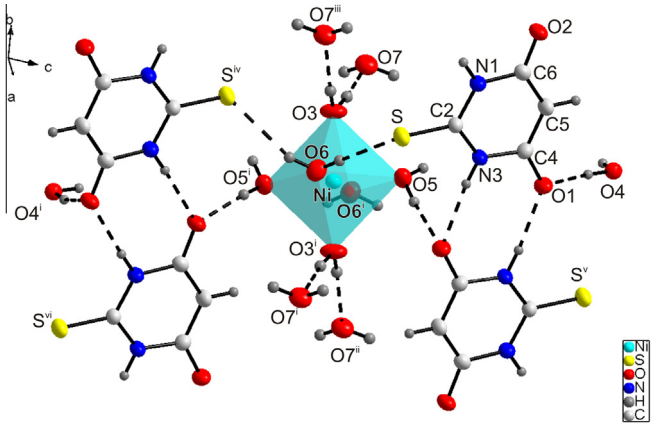

Fig. 1. NiO_6 octahedral coordination in **1** together with the numbering scheme. Symmetry code: (i) 1 −*x*, −*y*, −*z*; (ii) *x*, −1 + *y*, *z*; (iii) 1 −*x*, 1 − *y*, −*z*; (iv) −*x*, −*y*, −*z*; (v) 1 −*x*, −*y*, 1 − *z*; (vi) *x*, −1 + *y*, −1 + *z*. The ellipsoids are drawn at the 50% probability level, dashed lines indicate H-bonds.

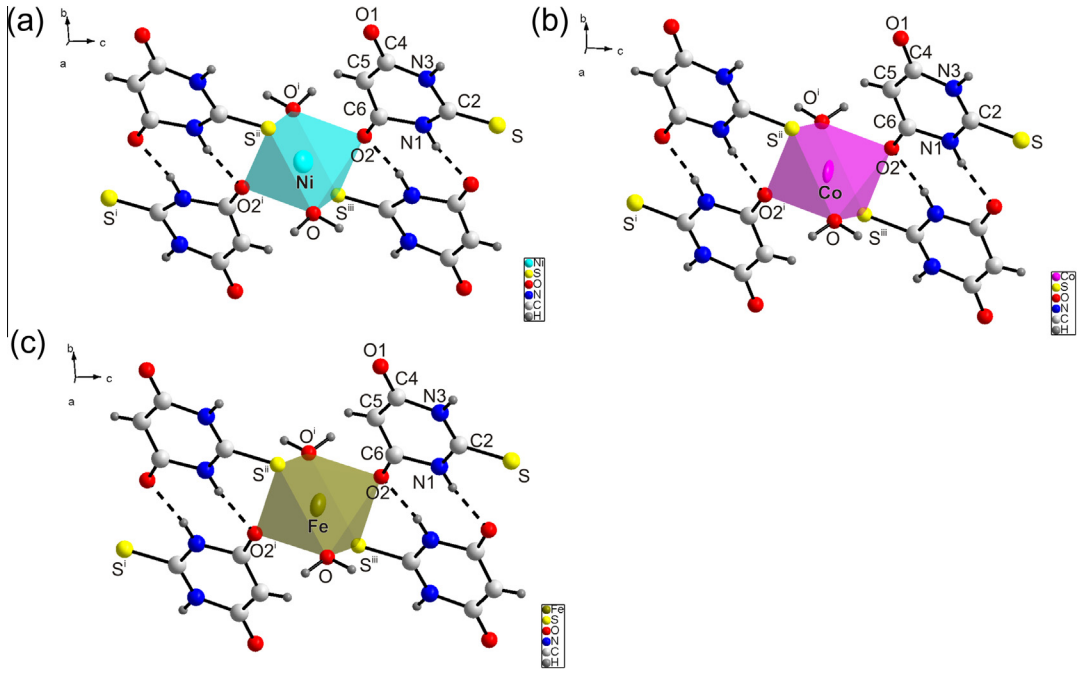

Fig. 2. The crystal structures of (a) **2**; (b) **3**; (c) **4** together with the numbering scheme. Symmetry code: (i) 2 −*x*, −*y*, −*z*; (ii) *x*, *y*, −1 + *z*; (iii) 2 −*x*, −*y*, 1−*z*. The ellipsoids are drawn at the 50% probability level.

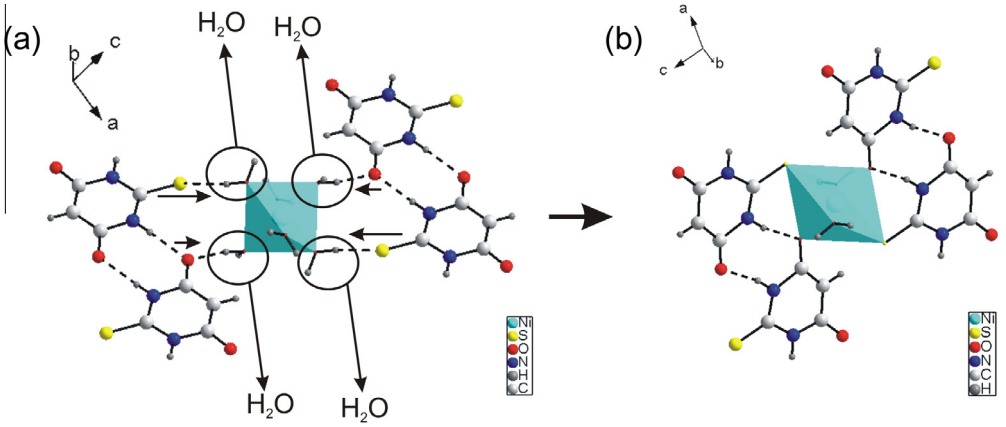

Fig. 3. (a) Precursor **1** looses four coordinated H_2O molecules and the $HTBA^-$ ions move towards Ni(II); (b) the final crystal structure of **2** after the reconstruction of the precursor **1**.

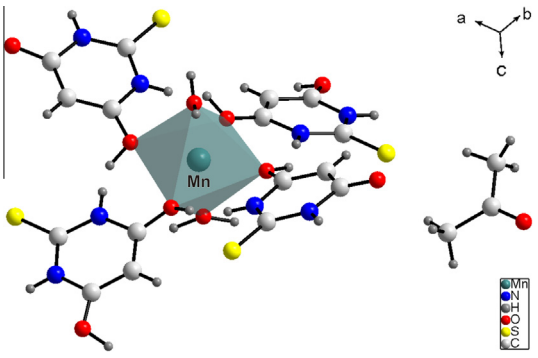

Fig. 4. The crystal structure of $\{[Mn(H_2O)(HTBA)_2)]\cdot 2(OC_3H_6)\}_n$ [15].

water molecules (Fig. 1, 3a and Fig. 5S). Complex **2** is formed by the substitution of four water molecules in $Ni(H_2O)_6^{2+}$ by two O- and two S-coordinated $HTBA^-$ ions (Fig. 3).

Up until now, structures of 2-thiobarbiturate complexes with the d-metal ions Mn(II), Zn(II) [16], Au(I) [23], Co(III) [24] and Cd(II) [21] have been determined. In $\{[M(H_2O)(HTBA)_2)]\cdot 2(OC_3H_6)\}_n$ (M = Zn, Mn) [16], the metal is connected only to four oxygen atoms, coming from four $HTBA^-$ ligands (Fig. 4), but in compounds **2**–**4** the metal is connected with oxygen and sulfur atoms. The deprotonation of the nitrogen atom is found, as expected, only in highly alkaline solutions or in the case of complex formation with metal ions possessing a high affinity for nitrogen, such as Au (I) [23] and Co (III) [24].

Like in **1** and **2**–**4**, the hydrogen bonds N1–H1···O2, N3–H3···O1, O–H2···O1 and O–H4···O1 close 8-membered rings $R_2^2(8)$. The distances between the rings centers of neighboring

Table 3
Characteristic IR bands (cm^{-1}) of **2**–**4**.

Assignment	H_2TBA	Complex **2**	Complex **3**	Complex **4**
ν(O–H)	–	3394	3364	3338
ν(N–H), ν(C–H)	3096–2871	3113–2870	3108–2868	3107–2869
ν(C=O)	1719	1626	1625	1624
ν(C=O)	1646	1594	1592	1589
ν(NHC=S)	1567	1560	1560	1560
ν(C=S)	1162	1200	1201	1202

$HTBA^-$ ions are equal to 3.428(5) (**2**), 3.411(7) (**3**) and 3.433(7) Å (**4**), therefore there are π–π interactions between the rings (Fig. 8S), contrary to that in **1**. The π–π stacking is of the head-tail type [25], as in the isostructural $Cd(H_2O)_2(HTBA)_2$ [21]. In K(I) [17,18] and Pb(II) [19] HTBA complexes, the $HTBA^-$ ions display head-to-head packing.

3.3. IR spectroscopy

The vibrational spectra for solid H_2TBA and **2**–**4** dispersed in the KBr pellet were recorded in the range 4000–400 cm^{-1} and are shown in Figs. 9S–12S. The bands obtained for H_2TBA are virtually identical with those reported by Mendez et al [26] for solid H_2TBA (enol form, N10). The assignment of the IR vibrational bands to the corresponding normal modes is based on the data reported for thiobarbituric acid [26–28]. The presence of the signal corresponding to the cyclic thioamide structure NH (C=S) at 1567 cm^{-1} (Table 3) indicates that the thione form prevails in the solid state. The band found at 3096–2871 cm^{-1} in the infrared spectrum was assigned to the ν(CH) stretching mode of the R2C=CHR pseudo-vinyl structure of the enol tautomer of H_2TBA [28] and ν(N–H) [26]. In addition, the characteristic bands at 1719 and 1646 cm^{-1}, attributed to the carbonyl group in the β-unsaturated position, are in agreement with the presence of the N10 isomer in the solid state [26,27]. The changes in the position and intensity of these bands indicate that at least one of two O atoms of the carbonyl groups in the 2-thiobarbituric acid is coordinated to Fe(II), Co(II) or Ni(II). The characteristic bands at 1567 and 1162 cm^{-1}, previously assigned to ν(C=S) stretching [26,27], are shifted in the spectra of **2**–**4**, which means that the C=S group is involved in coordination to the metal ions. The broad bands at 3338-3394 cm^{-1} in the IR spectra of **2**–**4** are due to ν(O–H) of coordinated water molecules involved in the hydrogen-bonding interactions.

3.4. Thermal decomposition

A thermal decomposition study of the 2-thiobarbituric acid complexes has been carried out to corroborate the information obtained from their structural data about the status of water molecules present in these complexes, as well as to know their general decomposition patterns.

For **4**, the initial weight loss takes place at 40–280 °C (Fig. 13Sa). It is mainly associated with water production and some amount of carbon and sulfur oxides, and this process is accompanied by a weak exo-effect. Both the TG and DSC curves show a one-step dehydration which overlaps partially with the start of the organic moiety oxidation. Most probably, this overlap accounts for the observed difference between the experimental value of the weight loss (13.2%) and the expected value (9.52%) for the removal of two water molecules (Table 2). The exothermic oxidative degradation of the organic moiety at 300–480 °C results in H_2O, CO_2, SO_2 and NO evolution without the formation of definite products. Almost no water production was found at temperatures above 450 °C, and carbon dioxide and NO are predominantly formed along with a very sharp heat evolution at 450–465 °C. Finally, on being heated to 900 °C, the sample undergoes the complete transformation to α-Fe_2O_3, according to the XRD analysis (Fig. 14S). The total weight loss Δm_{obs} (Fig. 13Sa, Table 2) was found to be 78.93%, and this value is very close to the expected Δm_{clc} of 78.88% for $Fe(H_2O)_2(HTBA)_2$ to ½ Fe_2O_3 conversion.

Co_3O_4 (Fig. 15S) was found to be the final product for the oxidative decomposition of $Co(H_2O)_2(HTBA)_2$. The observed weight loss Δm_{obs} of 78.02% satisfactorily fits the theoretical value of 78.95% (79.48% and 80.35%, accordingly for CoO, Table 2). Similar to **4**, the overlap of the dehydration and decomposition stages leads to a substantial excess of Δm_{obs} over Δm_{clc} (Table 2). The main difference between $Fe(H_2O)_2(HTBA)_2$ and $Co(H_2O)_2(HTBA)_2$ is that the oxidation of the organic moiety of the latter occurs gradually at higher temperatures (Figs. 13Sa,b). The maxima of the thiobarbiturate oxidation rates were observed at 460 °C (Fe) and 500 °C (Co), the width of the DSC peaks being 6–7 and 40–50 °C, respectively.

The thermoconversion of $Ni(H_2O)_2(HTBA)_2$ results in NiO formation (Fig. 16S). The total weight loss Δm_{obs} of 79.8% is slightly less than the expected value Δm_{clc} of 80.39%. The general behavior of the thermoconversion of **2** is similar to that of the iron salt and is characterized by a dehydration process corresponding to a pronounced endothermic DSC peak at around 270 °C, subsequent long-tailed weight-loss steps in the temperature region up to 500 °C and a very sharp exothermic DSC peak with a top temperature of 510 °C (Fig. 13Sc).

There was not clear correlation observed between T_m (the temperature of the dehydration rate maximum) and the nature of the metal. In general, for $Co(H_2O)_2(HTBA)_2$, the T_m value of the dehydration step is slightly lower and that of the oxidation stage is higher than the T_m values for the Fe(II) and Ni(II) salts. The metal oxides (Fe_2O_3, Co_3O_4 and NiO) are the final thermoconversion products. Some discrepancy between the experimental and calculated weight loss found for the Co(II) and Ni(II) complexes may be attributed to the presence of a small amount of impurities (up to 3%), most likely from the starting materials.

At present, the thermal behavior of metal 2-thiobarbiturates is insufficiently described in the literature. The studies are not systematic and cover only a few complexes of Cu(I) [29], Cr(III), Mo(V) [30], Fe(II), Fe(III), Co(II), Cu(II), Zn(II) and Cd(II) [31]. It should be noted that in the present work, the synthesized compounds of Fe(II) and Co(II) are different in composition from the previously known ones [31]. Studies [29–31] were performed under non-oxidative conditions (flowing nitrogen) and nothing is known about the peculiarities of the thermal conversion in the presence of oxygen. According to the TG and DSC data (Fig. 13S, Table 2), the studied substances are thermally stable under oxidative conditions, at least up to 130 °C. The decomposition process of $M(H_2O)_2(HTBA)_2$ (M = Fe, Co, Ni) under oxidative conditions may be divided into three major stages: dehydration, oxidative degradation of the organic moiety and transformation of the inorganic residue. The same sequence of thermal decomposition steps was observed for the thiobarbiturates of other metals [29–32].

4. Conclusions

Four new compounds, the discrete complex $[Ni(H_2O)_6](HTBA)_2{\cdot}2H_2O$ (**1**) and three coordination polymers $M(H_2O)_2(HTBA\text{-}O,S)_2$, M = Ni (**2**), Co (**3**) and Fe (**4**), were synthesized and structurally characterized. Blue single crystals of **1** precipitate in solution at 5–20 °C as a precursor to **2**, and then quickly decompose into the yellow powder $Ni(H_2O)_2(HTBA)_2$ (**2**). The structure of **1** contains almost an ideal octahedral $Ni(H_2O)_6^{2+}$ cation, and there is no coordination of Ni(II) by $HTBA^-$. Complexes **2-4** are isostructural polymers where each metal ion is surrounded by two

water molecules, two O-coordinated $HTBA^-$ ions and two S-coordinated $HTBA^-$ ions in *trans*-positions and has an octahedral geometry. These complexes are also isostructural with the previously reported $Cd(H_2O)_2(HTBA)_2$ [21]. These octahedrons connect μ_2-O,S bridging ligands. The dependence of the cell volume on the ion radius of the Me(II) ions of **2**, **3**, **4** and $Cd(H_2O)_2(HTBA)_2$ show a good linear correlation. The crystal structures of **1**–**4** are stabilized by numerous hydrogen bonds. The crystal structures of **2**–**4** are also stabilized by π–π stacking interactions of the head-tail type. Infrared spectroscopy also evidenced the complex formation. The studied substances are thermally stable under oxidative conditions at least up to 130 °C. The thermal decomposition at higher temperatures may be divided into three major stages.

Appendix A. Supplementary data

CCDC 966580, 966595, 966598 and 966599 contains the supplementary crystallographic data for **1**–**4**. These data can be obtained free of charge via http://www.ccdc.cam.ac.uk/conts/retrieving.html, or from the Cambridge Crystallographic Data Centre, 12 Union Road, Cambridge CB2 1EZ, UK; fax: (+44) 1223-336-033; or e-mail: deposit@ccdc.cam.ac.uk. Supplementary data associated with this article can be found, in the online version, at http://dx.doi.org/10.1016/j.poly.2013.12.021.

References

[1] E.S. Raper, Coord. Chem. Rev. 165 (1997) 475.
[2] S. Bondock, El-Gaber Tarhouni, A.A. Fadda, Phosphorus, Sulfur Silicon Relat. Elem. 182 (2007) 1915.
[3] D.J. Tranchemontagne, J.L. Mendoza-Cortes, M. O'Keeffe, O.M. Yaghi, Chem. Soc. Rev. 38 (2009) 1257.
[4] S. Natarajan, J.K. Sundar, S. Athimoolam, B.R. Srinivasan, J. Coord. Chem. 64 (2011) 2274.
[5] K. Biradha, A. Ramanan, J.J. Vittal, Cryst. Growth Des. 9 (2009) 2969.
[6] G.M. Sheldrick, SHELXS97 and SHELXL97, University of Göttingen, Germany, 1997.
[7] I.C. Madsen, R.J. Hill, Adv. X-Ray Anal. 35 (1992) 39.
[8] I.C. Madsen, R.J. Hill, J. Appl. Crystallogr. 27 (1994) 385.
[9] W.I.F. David, Abstract P2.6, NIST Special Publication 846 (1992) 210.
[10] Diffrac-Plus Basic XRD Wizard, 2002–2007 Bruker AXS GmbH, Karlsruhe, Germany.
[11] Bruker AXS TOPAS V4: General profile and structure analysis software for powder diffraction data – User's Manual, Bruker AXS, Karlsruhe, Germany, 2008.
[12] PLATON – A Multipurpose Crystallographic Tool. Utrecht University, Utrecht, The Netherlands, 2008.
[13] F.H. Allen, Acta Crystallogr., Sect. B 58 (2002) 380.
[14] M.-R. Calas, J. Martinez, C.R. Acad. Sci. Ser. C 265 (1967) 631.
[15] M.R. Chierotti, L. Ferrero, N. Garino, R. Gobetto, L. Pellegrino, D. Braga, F. Grepioni, L. Maini, Chem.-Eur. J. 16 (2010) 4347.
[16] Z.R. Pan, Y.C. Zhang, Y.L. Song, X. Zhuo, Y.Z. Li, H.G. Zheng, J. Coord. Chem. 61 (2008) 3189.
[17] M. Kubicki, A. Owczarzak, V.I. Balas, S.K. Hadjikakou, J. Coord. Chem. 65 (2012) 1107.
[18] N.N. Golovnev, M.S. Molokeev, Russ. J. Struct. Chem. 54 (2013) 521.
[19] N.N. Golovnev, M.S. Molokeev, Russ. J. Struct. Chem. 54 (2013) 940.
[20] N.N. Golovnev, M.S. Molokeev, Acta Crystallogr., Sect. C 69 (2013) 704.
[21] N.N. Golovnev, M.S. Molokeev, Russ. J. Inorg. Chem. 58 (2013) 1193, http://dx.doi.org/10.1134/S0036023613100094.
[22] R.D. Shannon, Acta Crystallogr., Sect. A 32 (1976) 751.
[23] W.J. Hunks, M.C. Jennings, R.J. Puddephatt, Inorg. Chem. 41 (2002) 4590.
[24] K. Yamanari, M. Kida, A. Fuyuhiro, M. Kita, S. Kaizaki, Inorg. Chim. Acta 332 (2002) 115.
[25] J.W. Steed, J.L. Atwood, Supramolecular Chemistry, first ed., CRC Press, 2004, IKTs Akademkniga, Moscow, 2007.
[26] E. Mendez, M.F. Cerda, J.S. Gancheff, J. Torres, C. Kremer, J. Castiglioni, M. Kieninger, O.N. Ventura, J. Phys. Chem. C 111 (2007) 3369.
[27] R.I. Bakalska, V.B. Delchev, Acta Chim. Slov. 59 (2012) 75.
[28] C.A. Téllez Soto, J.M. Ramos, A.C.J. Costa, L.S. Vieira, J.L. Rangel, L. Raniero, P.P. Fávero, T. Lemmaa, G.F. Ondar, O. Versiane, A.A. Martin, Spectrochim. Acta, Part A 114 (2013) 475.
[29] A. Jiménez, H. Jiménez, J. Borrás, Synth. React. Inorg. Met.-Org. Chem. 17 (1987) 159 (DOI: 0.1080/00945718708059421).
[30] M.S. Refat, S.A. El-Korashy, A.S. Ahmed, Spectrochim. Acta, Part A 71 (2008) 1084.
[31] Z.M. Zaki, G.G. Mohamed, Spectrochim. Acta, Part A 56 (2000) 1245.
[32] N.N. Golovnev, M.S. Molokeev, S.N. Vereshchagin, V.V. Atuchin, J. Coord. Chem. 66 (2013) 4119.